FEBS Letters 589 (2015) 45–51

FEBS Letters

journal homepage: www.FEBSLetters.org

c-di-AMP recognition by *Staphylococcus aureus* PstA

Martina Müller, Karl-Peter Hopfner, Gregor Witte *

Ludwig-Maximilians-Universität München, Gene Center and Dept. of Biochemistry, Feodor-Lynen-Str. 25, 81377 Munich, Germany

ARTICLE INFO

Article history:
Received 16 October 2014
Revised 13 November 2014
Accepted 13 November 2014
Available online 28 November 2014

Edited by Stuart Ferguson

Keywords:
Cyclic-di-AMP
P_{II}-related protein
Ferredoxin-like fold
Crystal structure
Bacterial signal transduction

ABSTRACT

Cyclic-di-AMP (c-di-AMP) is a bacterial secondary messenger involved in various processes, including sensing of DNA-integrity, cell wall metabolism and potassium transport. A number of c-di-AMP receptor proteins have recently been identified in *Staphylococcus aureus*. One of them - PstA - possesses a ferredoxin-like fold and is structurally related to the class of P_{II} signal-transduction proteins. P_{II} proteins are involved in a large number of pathways, most of them associated with nitrogen metabolism. In this study we describe the mode of c-di-AMP binding and subsequent structural changes of *S. aureus* PstA. An altered architecture in PstA compared to canonical P_{II} proteins results in differences in ligand coordination.

1. Introduction

Nucleotide secondary messengers are key components of the signal transduction networks that link sensory input signals to the responses of the cell. The most prominent examples in bacteria are cyclic AMP and (p)ppGpp, both of which control genome wide expression. The cyclic di-nucleotide messenger molecule c-di-GMP acts as a "lifestyle" signal, regulating biofilm formation, cell cycle progression, development and virulence. In the past few years two new members of bacterial nucleotide messengers have been identified, namely c-di-AMP and 3,3-cGAMP. The latter is little characterized but it has been shown to play a role in *Vibrio cholerae* gastrointestinal colonization [1] and is related to the 2,3-cGAMP synthesized by the eukaryotic innate immune DNA sensor cGAS [2,3]. The identification of c-di-AMP in 2008 [4] started a struggle for the identification of c-di-AMP related signaling pathways [5] and we are still at the beginning of understanding how c-di-AMP signaling is initiated, how the signal is transduced and which cellular processes are finally regulated. After the initial discovery of c-di-AMP in the crystal structure of *Thermotoga maritima* DisA [4], more diadenylate cyclase (DAC) domain proteins have been identified in a variety of bacteria [6–10]. Different functions were assigned to c-di-AMP signaling and it has been shown that deletion of all DAC domain proteins is lethal in *Bacillus subtilis* [9]. On the one hand, DNA damage or subsequent post-repair/recombination states of the DNA result in a reduced level of c-di-AMP due to inhibition of DisA, leading to sporulation delay in *B. subtilis* [11]. On the other hand, c-di-AMP has been reported to be involved in cell wall homeostasis [12], fatty acid synthesis [13] and potassium transport [14]. Aside from the DAC domain synthesizing c-di-AMP [4,15], there is little structural information about c-di-AMP degradation by the phosphodiesterase GdpP [16,17] or c-di-AMP-binding receptors. To date, six c-di-AMP receptors have been identified: the transcription factor DarR from *Mycobacterium smegmatis* [13]; ydaO riboswitches [18–20]; the potassium transport associated proteins KtrA and KdpD; the P_{II}-like protein PstA from the pathogen *Staphylococcus aureus* [14]; and the well-characterized protein pyruvate carboxylase, which was unexpectedly shown in a recent structural and biochemical study to be allosterically regulated by c-di-AMP [21].

The fact that c-di-AMP binds to PstA implies that the cyclic dinucleotide might also be involved in regulation of metabolism. PstA shares a ferredoxin-like fold with proteins of the P_{II} signal transduction family, which are omnipresent in bacteria, archaea and plants, and probably belong to the most widespread signal transducing proteins in nature. P_{II} proteins are mainly involved in the regulation of central metabolic processes and in particular cellular nitrogen metabolism (e.g. reviewed in [22]). After sensing of a ligand such as 2-oxoglutarate (2-OG) and/or adenosine nucleotides, P_{II} proteins regulate target proteins via protein–protein interactions with transcription factors, membrane transporters

* Corresponding author. Fax: +49 (0)89 2180 76999.
E-mail address: witte@genzentrum.lmu.de (G. Witte).

http://dx.doi.org/10.1016/j.febslet.2014.11.022

and different enzymes. All P_{II} proteins are trimers and consist of three identical subunits with an approximate molecular weight of 12–13kDa each. P_{II} proteins have a compact core domain with a double βαβ-architecture (ferredoxin-like fold) and inter-subunit clefts for ligand binding. Additional structural features are one large protruding loop (T-loop), a smaller B-loop and a C-terminal loop (C-loop). Whereas the latter are involved in ligand binding, the T-loop is flexible and rarely visible in crystal structures. However, the intrinsic flexibility is probably needed for regulatory protein–protein interactions. In bacteria, the T-loop is often post-translationally modified through uridylation of Tyr51 with effects on the signal transduction. All three ligand binding sites can bind one nucleotide and one 2-OG molecule each. While ATP binding is cooperative with 2-OG, ATP and ADP bind competitively and ADP acts antagonistic to 2-OG. The crystal structure of *Azospirillum brasilense* GlnZ in complex with ATP, 2-OG and a Mg^{2+} ion [23] was the first complex structure to shed light on the mode of ligand binding. Both ATP and 2-OG are bound in the inter-subunit cleft and, together with conserved residues in the binding cleft, coordinate the Mg^{2+} ion.

We solved the crystal structures of *S. aureus* PstA with and without its ligand c-di-AMP and were thus able to analyze the coordination of c-di-AMP and subsequent structural changes in PstA. The overall architecture of PstA differs from P_{II} proteins with respect to the protruding loops that are involved in interactions with both ligands and targets. In agreement with other structures of P_{II} proteins, c-di-AMP is bound in the inter-subunit clefts. In contrast, however, these clefts are closed by the small T-loops bending upwards and not the C-loops as previously observed.

2. Materials and methods

2.1. Cloning, expression and protein purification

S. aureus PstA (SACOL0525) was cloned into the pET28a expression vector via NdeI and NotI restriction sites. His_6-tagged PstA was expressed in *E. coli Rosetta* BL21(DE3) cells grown in LB. After reaching an OD_{600} of 0.6, expression was induced by addition of 0.2 mM IPTG and the temperature was lowered to 18 °C. Cells were harvested after 18 h and lysed in buffer A (50 mM Tris–HCl, 300 mM NaCl, 10 mM Imidazole, 10% v/v Glycerol, pH 7.5) via sonication. The cell lysate was cleared by centrifugation and loaded onto a Ni–NTA column (Qiagen). After washing with buffer A and buffer B (50 mM Tris–HCl, 300 mM NaCl, 40 mM Imidazole, 10% v/v Glycerol, pH 7.5) the protein was eluted with buffer C (50 mM Tris–HCl, 300 mM NaCl, 250 mM Imidazole, 5% v/v Glycerol, pH 7.5). PstA was dialyzed against buffer D (50 mM Tris–HCl, 100 mM NaCl, 5% v/v Glycerol, pH 7.5) and loaded onto a HiTrap Q HP (GE Healthcare). A linear gradient to 100% buffer E (50 mM Tris–HCl, 1 M NaCl, 5% v/v Glycerol, pH 7.5) was used to elute the protein. PstA-containing fractions were pooled, concentrated and loaded onto a HiLoad Superdex 75 column (GE Healthcare) equilibrated with running buffer F (20 mM Tris–HCl, 150 mM NaCl, 5% v/v Glycerol, pH 7.5). The PstA peak fractions were concentrated to 6 mg/ml and flash-frozen in liquid nitrogen for later use.

2.2. Crystallization, data collection and structure refinement

S. aureus PstA crystals were grown by hanging drop vapor-diffusion at 20 °C. Crystals were obtained by mixing 2 μL of protein (6 mg/ml) and 1 μL reservoir solution (55% v/v MPD, 0.1 M sodium acetate pH 4.3, 10 mM calcium chloride) with a total reservoir volume of 300 μL in the well. For co-crystallization of PstA with c-di-AMP, 1 μL of protein (6 mg/ml) supplemented with 0.75 mM c-di-AMP was mixed with 1 μL of reservoir solution (6% w/v PEG 8000, 0.1 M HEPES/NaOH pH 7.0, 0.2 M calcium acetate) with a reservoir volume of 300 μL. Crystals were flash-cooled in liquid nitrogen either directly from their mother liquor or after transfer into mother liquor supplemented with 25% v/v PEG 400 as a cryo-protectant (for crystals with c-di-AMP). Diffraction data were collected at the Swiss Light Source (Paul-Scherrer institute, Villigen, Switzerland) at the beamline X06SA at 100 K. Diffraction data were indexed and scaled using XDS/XSCALE [24]. The structure was determined by molecular replacement using PHASER [25] within the CCP4 package [26] using *Pediococcus pentosaceus* P_{II}-like protein (PDB code 3m05) as search model. Structure refinement comprised cycles of manual model building/refinement steps with Coot [27] and automatic refinement using PHENIX [28]. The data collection and refinement statistics are shown in Table 1. Coordinates and structure factors have been deposited in the Protein Data Bank as 4wk1 and 4wk3. All figures were prepared using PyMOL [29].

2.3. Size-exclusion coupled right-angle laser light scattering (SEC-RALS)

SEC-RALS data were collected using a Malvern/Viscotek system (TD270 RALS- and VE3580 RI-detector) connected to an ÄKTAmicro system equipped with a Superdex 200 Increase (10/300) column (GE Healthcare). To calibrate the system BSA (66kDa) was used. Data were evaluated with the OmniSEC software supplied with the instrument.

2.4. Surface plasmon resonance experiments

Surface plasmon resonance experiments to analyze binding of c-di-AMP to *S. aureus* PstA were performed using a Biacore X100+ system (GE Healthcare). *S. aureus* PstA was coupled to a CM-5 chip via amine coupling chemistry and free activated groups were inactivated using ethanolamine. To increase the sensitivity of the nucleotide binding we saturated the chip surface with PstA (5800 RU). Kinetic data were recorded for injections of c-di-AMP (and other nucleotides) in HBS-EP buffer (150 mM NaCl, 10 mM HEPES/NaOH pH 7.4, 3 mM EDTA, 0.05% P-20). Data from an empty flow cell (FC1) were subtracted as reference to correct for unspecific binding of the analytes to the chip surface. Data were analyzed using the Biacore X100 Evaluation software.

2.5. Thermal shift assays

Thermal stability of PstA in presence of ligands was probed using fluorescence thermal shift assays [30]. 19 μM PstA (+1 mM ligand) in 50 mM Tris–HCl pH 7.5, 150 mM NaCl, 5% v/v glycerol, 5 mM $MgCl_2$ with SYPRO orange (final concentration 4x, Invitrogen) was analyzed in a real-time PCR machine. After equilibration at 5 °C for 30 s the melting curve was measured using a gradient with 0.5 K/30 s from 5 °C to 100 °C and one scan/0.5 K.

2.6. Differential radial capillary action of ligand assay

DRaCALA assays were performed as e.g. described in [14]. 20 μM *S. aureus* PstA or the control ATP-binding protein (human nucleotidyl transferase) in assay buffer (50 mM Tris–HCl pH 7.5, 150 mM NaCl, 5 mM $MgCl_2$) were incubated for 5 min with different concentrations of ATP-α^{32}P (1–10 nM). 3.5 μL of the reaction mixture were spotted on a nitrocellulose membrane, dried and radioactivity was detected using a phosphor-imaging system (GE Healthcare).

Table 1
Crystal parameters, data collection and refinement statistics for *S. aureus* PstA.

Crystal data	PstA	PstA + c-di-AMP
Space group	$P4_332$	H32
Molecules per ASU	1	1
Unit cell parameters		
a, *b*, *c* (Å)	99.32, 99.32, 99.32	68.1, 68.1, 135.74
α, β, γ (°)	90, 90, 90	90, 90, 120
Data collection statistics		
Diffraction source	SLS beamline X06SA	SLS beamline X06SA
Wavelength (Å)	0.99998	0.99998
Data processing statistics		
Resolution range (Å)	70.23–2.60 (2.67–2.60)	50–1.98 (2.03–1.98)
No. of observed reflections	701 580 (14290)	141 089 (2745)
No. of unique reflections	5565 (392)	8523 (512)
Completeness (%)	99.9 (99.2)	97.7 (81.4)
Multiplicity	36.2 (36.1)	16.6 (5.4)
$I/\sigma I$	33.1 (2.5)	23.6 (2.0)
R_{meas} (%)	7.0 (198)	7.4 (105.3)
Refinement		
Resolution (Å)	44.42–2.60	44.52–1.98
No. of used reflections	5563	8522
R_{work} (%)/R_{free}[a] (%)	25.2/29.2	18.8/22.9
No. of atoms (total)	598	779
Protein	593 (77 residues)	703 (92 residues)
Ligand	1	1 (Ca^{2+}); 43 (c-di-AMP)
Water	4	23
Average B factors (Å^2)		
Wilson B factor	85.36	42.75
Overall	98.12	54.3
Protein	98.11	54.3
Ligands/water	Cl^- 129.5/89.6	c-di-AMP 49.1; Ca^{2+} 70.7/54.2
R.M.S. deviations		
Bond lengths (Å)/angles (°)	0.009/1.18	0.008/1.20
Ramachandran plot analysis		
Favoured (%)	98.6	98.9
Allowed (%)	1.4	1.1
Disallowed (%)	0	0
PDB identifier	4wk3	4wk1

Values in parentheses are for the highest resolution shell.
[a] 10% of the total number of reflections were used for the R_{free} calculations.

3. Results and discussion

The *S. aureus* protein PstA has a ferredoxin-like fold and its core domain shares the highly conserved architecture of the GlnB/K P_{II} proteins to which it is structurally closely related. A comparison of the secondary structure of PstA with canonical P_{II} proteins (e.g. *E. coli* GlnK), however, clearly shows that the lengths of the loops are exchanged (Fig. 1A). The loop connecting the double βαβ-motif comprises only 8 amino acids and is thus substantially shorter than the approximately 20 residue long T-loop typically present in this domain. Vice versa, the 33 residue long B-loop in the vicinity of the ligand binding cleft is significantly larger in *S. aureus* PstA than the eight residue loop in GlnK. The carboxy-terminal C-loop that usually covers the ligand binding cleft is absent in *S. aureus* PstA. As the overall properties of PstA deviate from previously described P_{II} proteins, we first analyzed the biochemical properties of PstA in solution to exclude the possibility that the protein forms different oligomers to the canonical trimeric P_{II} proteins. We thus performed size-exclusion chromatography coupled right-angle light scattering (SEC-RALS) experiments to determine the molecular weight in solution (Fig. 1B and C). Both the SEC-RALS data and the molecular weight determined from the hydrodynamic radius in size-exclusion chromatography show that PstA is a monodisperse trimeric species in solution ($Mw^{theoretical\ (trimer)}$ = 42kDa, $Mw^{SEC\text{-}RALS}$ = 43kDa, Mw^{SEC} = 47kDa). The fact that the apparent molecular weight from size-exclusion chromatography is higher than the molecular weight determined by light scattering is probably due to the protruding loops in PstA. Flexible regions lead to an increase in hydrodynamic radius and thus to a larger retention volume than a globular protein of the same size.

3.1. Binding of c-di-AMP

To probe binding of small molecules we measured the thermal stability of PstA in absence and presence of putative regulatory ligands using fluorescence-based thermal shift assays (TSA). In good agreement with P_{II} proteins [31], PstA shows a remarkably high thermal stability with an approximate melting temperature of 74.5 °C under the conditions used. Since ligand binding usually increases the melting temperature of a protein, we analyzed the melting behavior of PstA in the presence of nucleotides and/or 2-oxoglutarate (2-OG, α-ketoglutaric acid). While guanosine and non-cyclic adenosine nucleotides do not alter the melting temperature, c-di-AMP shifts the melting temperature of PstA by approximately 19 °C to 93.5 °C, indicating a remarkable gain in stability caused by a higher number of interactions within the complex. These observations are in good agreement with experiments by Corrigan et al. [14] that showed binding of c-di-AMP, but not other nucleotides, in differential radial capillary action of ligand assays (DRaCALA). The addition of 1 mM 2-OG had no detectable effect on the melting behavior of PstA.

In order to quantify the affinity and kinetic properties of c-di-AMP binding to PstA, we performed surface plasmon resonance (SPR) experiments. Amino-reactive coupling chemistry was used

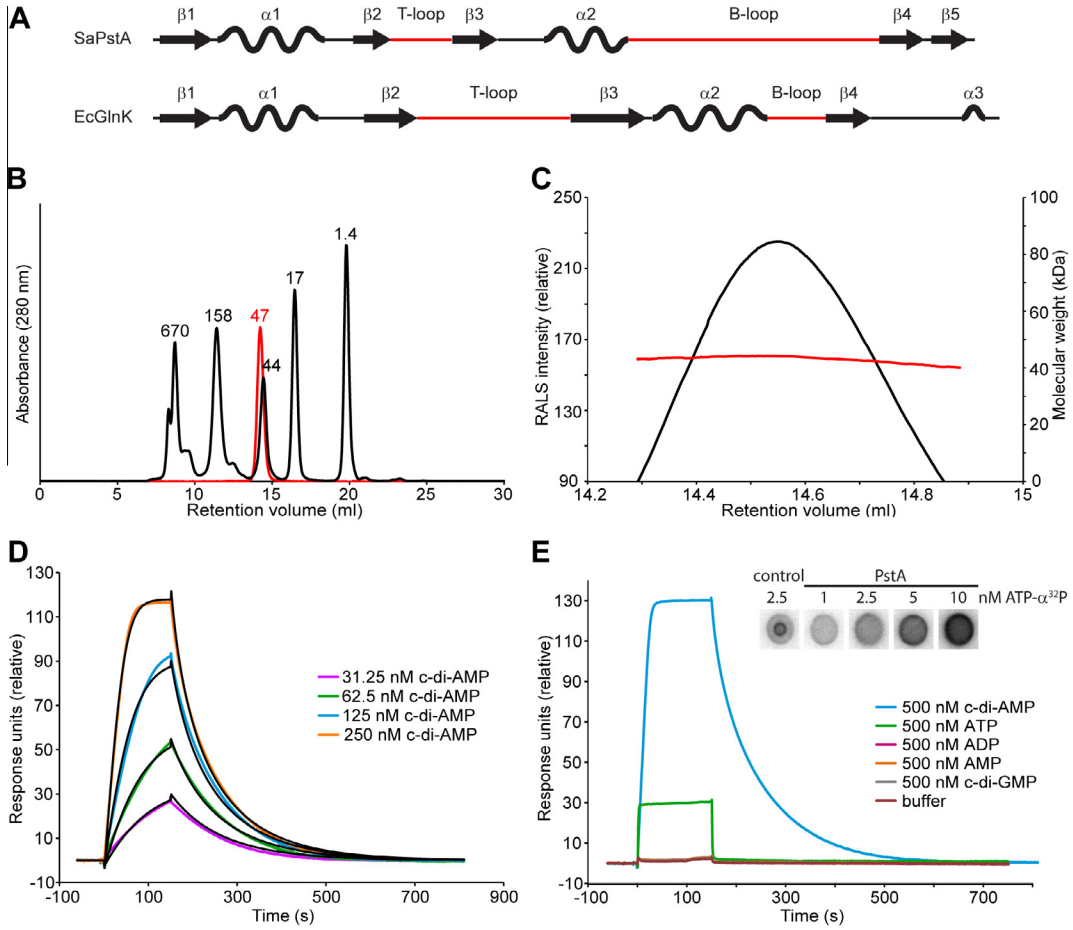

Fig. 1. Biochemical analysis of *S. aureus* PstA. (A) Comparison of the secondary structure of *S. aureus* PstA with a member of the canonical P_{II} protein family (*E. coli* GlnK). The lengths of the T- and B-loops are swapped in PstA compared to GlnK. (B) Size-exclusion chromatogram of a PstA sample (red curve) loaded onto a Superdex 200 Increase column and a molecular weight standard shown in black (peaks labeled with the respective masses of the proteins in kDa). Mw^{SEC}(PstA) = 47kDa was calculated using a calibration curve generated from the Mw-standard. (C) SEC-RALS curve of a PstA peak on the same column as in B. The molecular weight determined by RALS is constant for the entire PstA peak, indicating a monodisperse sample with a molecular weight of $Mw^{SEC\text{-}RALS}$ = 43kDa ($Mw^{theoretical\ (trimer)}$ = 42kDa). (D) Surface plasmon resonance (SPR) experiments. Injections of different concentrations of c-di-AMP (colored curves) over the immobilized *S. aureus* PstA chip-surface (FC2-1). The black curves show the fit of kinetic analysis with $k_a = 6.4 \times 10^5\ M^{-1}\ s^{-1}$, $k_d = 0.007\ s^{-1}$, RU_{max} = 173 for the binding of one c-di-AMP molecule to each PstA monomer. (E) Injections of different nucleotides show that ADP, AMP and c-di-GMP do not bind to PstA. ATP only binds to a small extent and this could not be confirmed in a DRaCALA assay. ATP binding is only observed in the positive control.

to covalently immobilize PstA to the chip surface and increasing concentrations of c-di-AMP (31.25–250 nM) in HBS-EP buffer were injected as the analyte (Fig. 1D). PstA displays robust binding of the cyclic di-nucleotide with K_D = 109 nM, an association rate of $k_a = 6.4 \times 10^5\ M^{-1}\ s^{-1}$ and a slow dissociation rate of $k_d = 0.07\ s^{-1}$. We also performed injections with ATP/Mg^{2+}, ADP, AMP, c-di-GMP and 2-OG (Fig. 1E). Only the ATP sample showed binding to PstA, albeit with much lower affinity, and no binding of AMP, ADP, c-di-GMP and 2-OG was detected under the conditions used. A combination of c-di-AMP and 2-OG resulted in comparable binding kinetics and K_D to c-di-AMP alone. The high affinity for c-di-AMP is mainly determined by the relatively fast on-rate and the slow dissociation kinetics. In comparison, the steep RU increase in ATP-binding sensorgrams indicates that both ATP binding and dissociation are much faster (beyond the sampling rate of the SPR instrument and thus $k_a \geqslant 10^7\ M^{-1}\ s^{-1}$), indicating that ATP-binding is energetically less favorable. A DRaCALA assay, however, did not show any binding of radioactively labeled ATP to PstA. Both the very fast on- and off-rates and weak binding observed in the SPR experiment indicate a transient interaction, which we deem unlikely to be of biological significance.

3.2. Crystal structures of PstA in absence and presence of c-di-AMP

To analyze the molecular details of c-di-AMP binding, we crystallized *S. aureus* PstA in the presence and absence of the cyclic dinucleotide. Apo PstA and c-di-AMP-PstA crystallized in the space groups $P4_332$ and H32, respectively, with one molecule per asymmetric unit. Both structures were solved by molecular replacement using the structure of *P. pentosaceus* PEPE_1480 (PDB code 3m05) as a search model, which we identified through homology searches using HHpred [32]. Traceable electron density covered 8 residues from the N-terminal purification tag and PstA residues 1–66 and 92–109 (numbers given for the complex structure). These residues mainly comprise the double βαβ-motif while the loop regions lacked traceable electron density and are thus likely to be flexible in the crystals (Fig. 2A). Statistics of data collection and model refinement are shown in Table 1. As suggested by the secondary structure comparison (Fig. 1A), the structure of PstA shows no obvious changes to the double βαβ-motif of the ferredoxin-like fold but the T- and B-loops are swapped in length with respect to canonical P_{II} proteins. Beta strands β1–β4 form the core of the PstA trimer while α-helices α1 and α2 are on the outside (Fig. 2A and B).

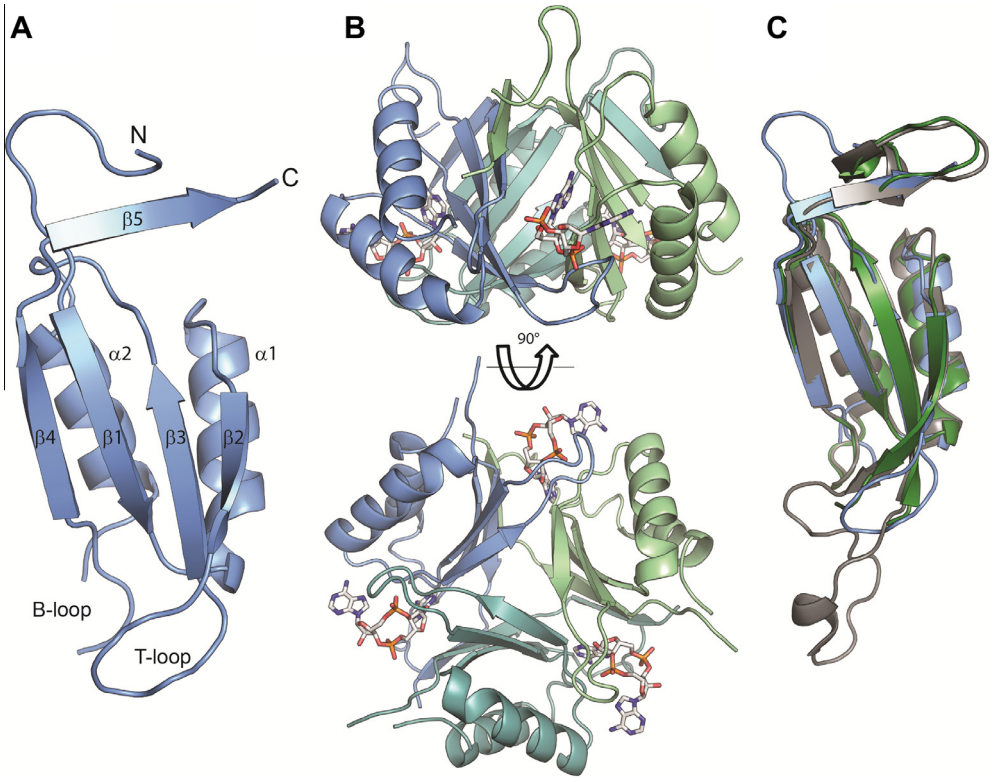

Fig. 2. Crystal structure of *S. aureus* PstA. (A) PstA monomer as present in the asymmetric unit. Residues in the B-loop region could not be traced in the electron density. The strand β5 extends the β-core domain of the neighboring PstA molecule by interacting with β4. (B) PstA trimer (approximate height 25 Å and diameter 40 Å) with bound c-di-AMP in side (upper part) and bottom views (lower part). The c-di-AMP moieties are deeply buried in the inter-subunit clefts. (C) Superposition of PstA and P_{II} proteins. The figure illustrates the structural similarity between *S. aureus* PstA (blue), *A. brasilense* GlnZ (PDB code 3mhy, grey, RMSD 1.18 Å) and *E. coli* GlnK (PDB code 2gnk, green, RMSD 0.854 Å).

The C-terminal β-strand β5 extends towards the neighboring subunit, where it interacts with β4 and thus stabilizes the trimer. The superposition of *S. aureus* PstA, *E. coli* GlnK and also *A. brasilense* GlnZ (Fig. 2C) reveals the high overall structural conservation of the ferredoxin-like core domains.

In the complex structure of PstA with c-di-AMP all three intersubunit binding clefts are occupied by the cyclic dinucleotide. The c-di-AMP moiety is almost completely buried in the binding cleft and is stabilized by a set of hydrophobic and ionic interactions. The binding cleft is clearly positively charged and almost perfectly matches the shape of the adenosine dinucleotide (Fig. 3A – electrostatic surface). Fig. 3B shows the c-di-AMP molecule with its respective electron density. The buried "inner" half of c-di-AMP is almost completely protected from the solvent area and coordinated by Asn-41, which forms a hydrogen bond with the 2′-hydroxyl group of the ribose, and additionally stabilized via a backbone interaction with Gly-47, which interacts with N^6 of adenine and thereby distinguishes between adenine and guanine cyclic dinucleotides. In comparison to the nucleotide free state, the small T-loop (residues 34–38), which is disordered in the apo state, becomes stabilized in the complex state and bends up towards the second "outer" adenine moiety. The base stacks with residues Phe-36 and Arg-26 and contributes to the extremely good coordination. This shielding and excessive ligand stabilization is in good agreement with the high binding affinity observed by surface plasmon resonance and the melting temperature shift in TSA. Interestingly, c-di-AMP shows a slower association rate than ATP, most probably due to the slower migration into the binding cleft that is just large enough to accommodate this molecule. To date, only one other protein complex with bound c-di-AMP has been reported, which is structurally very different [21] and we have not identified a common recognition motif for c-di-AMP.

3.3. Structural changes upon c-di-AMP binding and signal transduction

The overall structural changes between apo and complex states visible in the crystal structures are mainly short range movements in the core domain and the stabilization of the short T-loop (Fig. 3C and D). These structural changes upon ligand binding are supported by the fact that soaking of apo PstA crystals did not produce any diffracting crystals, possibly due to conformational changes disturbing the crystal lattice during binding of c-di-AMP. The high similarity of the apo and complex structures is reflected in a very low $RMSD_{overall}$ = 0.451 Å and also in the low per-residue RMSDs of the core domains (Fig. 3D). Because of the large amount of flexibility in the loop regions it is not possible to judge if any additional conformational changes in the B-loop occur in vivo. The loop regions have been shown to be crucial for signal transduction in all P_{II} proteins [22] but it is possible that PstA may function differently. Since we have no information on the structural changes of the B-loop due to lack of electron density, we can only speculate how PstA transduces signals, one option being that the longer B-loop instead of the T-loop mediates downstream signaling.

Fig. 3E shows a superposition of the structures of the P_{II} protein GlnZ from *A. brasilense* in complex with ATP/2-OG (PDB code 3mhy) and PstA in complex with c-di-AMP. The overall shape and surface properties are highly similar and the ATP and c-di-AMP binding clefts superpose closely. The "inner" base of c-di-AMP is almost in the same position as the ATP molecule in GlnZ. Interestingly, a second positively charged cavity in the direct

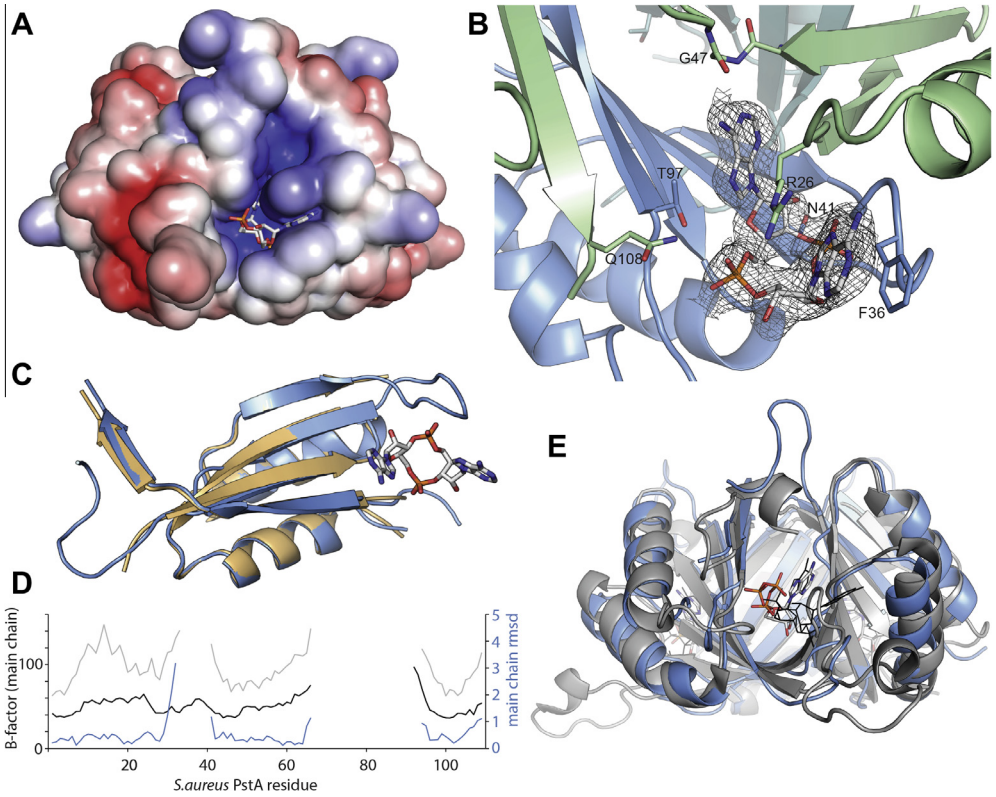

Fig. 3. Ligand binding. (A) PstA in solvent accessible electrostatic surface representation with c-di-AMP bound (blue = 5kT/e to red = −5kT/e). (B) Coordinated c-di-AMP molecule in the inter-subunit cleft with the corresponding electron density at 1σ (simulated annealing composite omit map). The "outer" adenine moiety is stacked by R26 and F36 while the "inner" adenine is specifically recognized at N^6 through a backbone interaction with G47. (C) Superposition of apo state PstA (shown in beige) and its c-di-AMP complex (shown in blue, RMSD 0.451 Å). Although no major structural changes in the overall architecture can be observed upon ligand binding, the T-loop becomes ordered and stabilizes the c-di-AMP moiety. (D) The plot shows the B-factors for the main chains of apo PstA (grey) and PstA-c-di-AMP complex (black) as well as the RMSD values for the Cα-atoms (blue curve, right axis) in the superposition of both structures (c.f. C). The T-Loop (residues 30–40) is clearly stabilized in the c-di-AMP complex. Additionally, the adjacent helix (residues 10–20) binds to the T-loop and thus has lower B-factors in the complex structure than in the apo structure. (E) Superposition of the PstA-c-di-AMP complex (blue) with GlnZ in complex with ATP/Mg^{2+}/2-OG (PDB code 3mhy, shown in grey, RMSD 1.18 Å). The "inner" adenine of c-di-AMP and ATP bound by GlnZ superimpose almost perfectly.

vicinity of the c-di-AMP binding pocket is visible in the electrostatic surface representation (Fig. 3A), which is sufficiently large to accommodate an additional small molecule ligand. As several structures of P_{II} proteins contain 2-OG close to ATP [23] bridged by a Mg^{2+} ion, this cavity might also be a binding site for a negatively-charged ligand. Even though our thermal shift assays and SPR experiments do not indicate binding of 2-OG by PstA under the conditions used, we cannot exclude the possibility that this ligand (or another small molecule) might bind in addition to c-di-AMP. From the structural point of view the second cavity would certainly allow accommodation of a ligand but its function remains to be analyzed in further studies.

We were able to structurally analyze c-di-AMP sensing by a signal transducing protein for the first time. Even though PstA shares its overall structural elements with canonical P_{II} proteins, significant differences, such as the swapped lengths of the B- and T-loops and the missing C-loop, result in altered ligand binding properties. Future research will show which target proteins are affected by PstA and the mechanism through which this occurs. This study substantially broadens our understanding of how c-di-AMP is recognized by target proteins.

Acknowledgements

We thank the staff of SLS X06SA for excellent onsite support and beamtime allocation, K. Lammens and D. Kostrewa for support with X-ray data, R. Byrne for comments on the manuscript and the Hopfner group for discussions. This work was funded by grants from the Deutsche Forschungsgemeinschaft (DFG) WI3717/2-1 to G.W. and GRK1721 to G.W. and K.-P.H., M.M. is supported by GRK1721.

Appendix A. Supplementary data

Supplementary data associated with this article can be found, in the online version, at http://dx.doi.org/10.1016/j.febslet.2014.11.022.

References

[1] Davies, Bryan W., Bogard, Ryan W., Young, Travis S. and Mekalanos, John J. (2012) Coordinated regulation of accessory genetic elements produces cyclic di-nucleotides for *V. cholerae* virulence. Cell 149, 358–370.
[2] Ablasser, A., Goldeck, M., Cavlar, T., Deimling, T., Witte, G., Rohl, I., Hopfner, K.P., Ludwig, J. and Hornung, V. (2013) CGAS produces a 2′-5′-linked cyclic dinucleotide second messenger that activates STING. Nature 498, 380–384.
[3] Gao, P., Ascano, M., Wu, Y., Barchet, W., Gaffney, B.L., Zillinger, T., Serganov, A.A., Liu, Y., Jones, R.A., Hartmann, G., Tuschl, T. and Patel, D.J. (2013) Cyclic [G(2′,5′)pA(3′,5′)p] is the metazoan second messenger produced by DNA-activated cyclic GMP-AMP synthase. Cell 153, 1094–1107.
[4] Witte, G., Hartung, S., Büttner, K. and Hopfner, K.P. (2008) Structural biochemistry of a bacterial checkpoint protein reveals diadenylate cyclase activity regulated by DNA recombination intermediates. Mol. cell 30, 167–178.
[5] Römling, U. (2008) Great times for small molecules: c-di-AMP, a second messenger candidate in Bacteria and Archaea. Sci. Signaling 1, pe39.
[6] Bai, Y., Yang, J., Zhou, X., Ding, X., Eisele, L.E. and Bai, G. (2012) Mycobacterium tuberculosis Rv3586 (DacA) is a diadenylate cyclase that converts ATP or ADP into c-di-AMP. PLoS ONE 7, e35206.

[7] Corrigan, R.M., Abbott, J.C., Burhenne, H., Kaever, V. and Gründling, A. (2011) C-di-AMP is a new second messenger in *Staphylococcus aureus* with a role in controlling cell size and envelope stress. PLoS Pathog. 7, e1002217.
[8] Kamegaya, T., Kuroda, K. and Hayakawa, Y. (2011) Identification of a *Streptococcus pyogenes* SF370 gene involved in production of c-di-AMP. Nagoya J. Med. Sci. 73, 49–57.
[9] Mehne, F.M., Gunka, K., Eilers, H., Herzberg, C., Kaever, V. and Stulke, J. (2013) Cyclic di-AMP homeostasis in bacillus subtilis: both lack and high level accumulation of the nucleotide are detrimental for cell growth. J. Biol. Chem. 288, 2004–2017.
[10] Woodward, J.J., Iavarone, A.T. and Portnoy, D.A. (2010) C-di-AMP secreted by intracellular Listeria monocytogenes activates a host type I interferon response. Science 328, 1703–1705.
[11] Oppenheimer-Shaanan, Y., Wexselblatt, E., Katzhendler, J., Yavin, E. and Ben-Yehuda, S. (2011) C-di-AMP reports DNA integrity during sporulation in *Bacillus subtilis*. EMBO Rep. 12, 594–601.
[12] Luo, Y. and Helmann, J.D. (2012) Analysis of the role of *Bacillus subtilis* sigma(M) in beta-lactam resistance reveals an essential role for c-di-AMP in peptidoglycan homeostasis. Mol. Microbiol. 83, 623–639.
[13] Zhang, L., Li, W. and He, Z.G. (2013) DarR, a TetR-like transcriptional factor, is a cyclic di-AMP-responsive repressor in *Mycobacterium smegmatis*. J. Biol. Chem. 288, 3085–3096.
[14] Corrigan, R.M., Campeotto, I., Jeganathan, T., Roelofs, K.G., Lee, V.T. and Gründling, A. (2013) Systematic identification of conserved bacterial c-di-AMP receptor proteins. Proc. Natl. Acad. Sci. U.S.A. 110, 9084–9089.
[15] Mehne, F.M., Schroder-Tittmann, K., Eijlander, R.T., Herzberg, C., Hewitt, L., Kaever, V., Lewis, R.J., Kuipers, O.P., Tittmann, K. and Stulke, J. (2014) Control of the diadenylate cyclase CdaS in *Bacillus subtilis*: an autoinhibitory domain limits cyclic Di-Amp production. J. Biol. Chem. 289, 21098–21107.
[16] Cho, K.H. and Kang, S.O. (2013) *Streptococcus pyogenes* c-di-AMP phosphodiesterase, GdpP, influences SpeB processing and virulence. PLoS ONE 8, e69425.
[17] Du, B., Ji, W., An, H., Shi, Y., Huang, Q., Cheng, Y., Fu, Q., Wang, H., Yan, Y. and Sun, J. (2014) Functional analysis of c-di-AMP phosphodiesterase, GdpP, in *Streptococcus suis* serotype 2. Microbiol. Res. 169, 749–758.
[18] Gao, A. and Serganov, A. (2014) Structural insights into recognition of c-di-AMP by the ydaO riboswitch. Nat. Chem. Biol. 10, 787–792.
[19] Nelson, J.W., Sudarsan, N., Furukawa, K., Weinberg, Z., Wang, J.X. and Breaker, R.R. (2013) Riboswitches in eubacteria sense the second messenger c-di-AMP. Nat. Chem. Biol. 9, 834–839.
[20] Ren, A. and Patel, D.J. (2014) C-di-AMP binds the ydaO riboswitch in two pseudo-symmetry-related pockets. Nat. Chem. Biol. 10, 780–786.
[21] Sureka, K., Choi, P.H., Precit, M., Delince, M., Pensinger, D.A., Huynh, T.N., Jurado, A.R., Goo, Y.A., Sadilek, M., Iavarone, A.T., Sauer, J.D., Tong, L. and Woodward, J.J. (2014) The cyclic dinucleotide c-di-AMP is an allosteric regulator of metabolic enzyme function. Cell 158, 1389–1401.
[22] Huergo, L.F., Chandra, G. and Merrick, M. (2013) P(II) signal transduction proteins: nitrogen regulation and beyond. FEMS Microbiol. Rev. 37, 251–283.
[23] Truan, D., Huergo, L.F., Chubatsu, L.S., Merrick, M., Li, X.D. and Winkler, F.K. (2010) A new P(II) protein structure identifies the 2-oxoglutarate binding site. J. Mol. Biol. 400, 531–539.
[24] Kabsch, W. (2010) Xds. Acta Cystallogr. Sect. D, Biol. Crystallogr. 66, 125–132.
[25] McCoy, A.J., Grosse-Kunstleve, R.W., Adams, P.D., Winn, M.D., Storoni, L.C. and Read, R.J. (2007) Phaser crystallographic software. J. Appl. Crystallogr. 40, 658–674.
[26] Winn, M.D., Ballard, C.C., Cowtan, K.D., Dodson, E.J., Emsley, P., Evans, P.R., Keegan, R.M., Krissinel, E.B., Leslie, A.G., McCoy, A., McNicholas, S.J., Murshudov, G.N., Pannu, N.S., Potterton, E.A., Powell, H.R., Read, R.J., Vagin, A. and Wilson, K.S. (2011) Overview of the CCP4 suite and current developments. Acta Cystallogr. Sect. D, Biol. Crystallogr. 67, 235–242.
[27] Emsley, P. and Cowtan, K. (2004) Coot: model-building tools for molecular graphics. Acta Cystallogr. Sect. D, Biol. Crystallogr. 60, 2126–2132.
[28] Afonine, P.V., Grosse-Kunstleve, R.W., Echols, N., Headd, J.J., Moriarty, N.W., Mustyakimov, M., Terwilliger, T.C., Urzhumtsev, A., Zwart, P.H. and Adams, P.D. (2012) Towards automated crystallographic structure refinement with phenix.refine. Acta Cystallogr. Sect. D, Biol. Crystallogr. 68, 352–367.
[29] L.L.C. Schrödinger, The PyMOL Molecular Graphics System, Version 1.3r1, 2010.
[30] Boivin, S., Kozak, S. and Meijers, R. (2013) Optimization of protein purification and characterization using Thermofluor screens. Protein Expression Purif. 91, 192–206.
[31] Moure, V.R., Razzera, G., Araujo, L.M., Oliveira, M.A., Gerhardt, E.C., Muller-Santos, M., Almeida, F., Pedrosa, F.O., Valente, A.P., Souza, E.M. and Huergo, L.F. (2012) Heat stability of Proteobacterial PII protein facilitate purification using a single chromatography step. Protein Expression Purif. 81, 83–88.
[32] Söding, J. (2005) Protein homology detection by HMM-HMM comparison. Bioinformatics 21, 951–960.